Electronic Supplementary Material (ESI) for Chemical Communications.
This journal is © The Royal Society of Chemistry 2023

Supporting Information

Aggregation induced circular polarized phosphorescence of chiral platinum(II) complex with BINOL ligand

Daiki Tauchi,[a] Taiki Koida,[a] Yuki Nojima,[b] Masashi Hasegawa,[b] Yasuhiro Mazaki,[b] Akiko Inagaki,[c] Ken-ichi Sugiura,[d] Yuki Nagaya,[e] Kazunori Tsubaki,[e] Takuya Shiga,[f] Yuuya Nagata,[g] Hiroyuki Nishikawa[a*]

[a]Graduate School of Science and Engineering, Ibaraki University, 2-1-1Bunkyo, Mito, Ibaraki 310-8512, Japan.
[b]Graduate School of Science, Kitasato University, 1-15-1 Minami-Ku, Kitasato, Sagamihara, Kanagawa 252-0373, Japan.
[c]Faculty of Science and Technology, Seikei University, 3-3-1 Kichijoji, Musashino, Tokyo 180-8633, Japan
[d]Graduate School of Science, Tokyo Metropolitan University, 1-1 Misami-Ohsawa, Hachioji, Tokyo 192-0397, Japan
[e]Graduate School of Life and Environmental Science, Kyoto Prefecture University, 1-5 Sakyo-Ku, Kyoto 606-8522, Japan.
[f]Faculty of Pure and Applied Sciences, University of Tsukuba, 1-1-1 Tennodai, Tsukuba 305-8577, Japan.
[g]Institute for Chemical Reaction Design and Discovery (WPI-ICReDD), Hokkaido University, Sapporo, Hokkaido 001-0021, Japan.

Table of Contents

General Information S3
Spectroscopy S3
Preparation of powder samples and PMMA films for the spectroscopy S4
X-ray crystallography S4

Theoretical calculation S4
General procedure for synthesis of *R*- and *S*-Pt S5
Figure S1. ^{1}H NMR spectrum of ***R*-Pt** S6
Figure S2. ^{1}H NMR spectrum of ***S*-Pt** S7
Figure S3. ^{13}C NMR spectrum of ***R*-Pt** S8
Figure S4. ^{13}C NMR spectrum of ***S*-Pt** S8
Figure S5. Mass spectrum of ***R*-Pt** S9
Figure S6. Mass spectrum of ***S*-Pt** S9
Figure S7. Crystal structure of ***S*-Pt** S10
Figure S8. Absorption spectrum of ***S*-Pt** in acetonitrile solution S12
Figure S9. Absorption spectra of ***R*-Pt** and ***S*-Pt** in PMMA films S12
Figure S10. Emission spectra of ***S*-Pt** in powder and PMMA film S13
Figure S11. Emission spectra of ***R*-Pt** in THF-water with different volume fraction of water S13
Figure S12. Emission spectra of ***S*-Pt** and ***R*-Pt** in PMMA films (f_{Pt} = 1, 2, 5 wt%) S14
Figure S13. CIE (x, y) coordinates of ***S*-Pt** in PMMA films (f_{Pt} = 1, 2, 5 wt%) S15
Figure S14. Emission spectra of ***R*-Pt** in various solutions S16
Figure S15. Dynamic light scattering profile of ***R*-Pt** and ***S*-Pt** in THF-water mixed solution (f_w = 95%) S17
Figure S16. Emission decay profile of ***S*-Pt** and ***R*-Pt** in powder and fit S18
Figure S17. Emission decay profiles of ***R*-Pt** and ***S*-Pt** in PMMA film (f_{Pt} = 1 wt%) and fit S18
Figure S18. g_{abs} and UV-vis spectra in acetonitrile, and g_{CPL} and emission spectra in powder of ***R*-Pt** and ***S*-Pt**. S19
Figure S19. CD and CPL spectra of ***S*-Pt** and ***R*-Pt** in PMMA film (f_{Pt} = 1 wt%) S20
Figure S20. CPL spectra of ***S*-Pt** and ***R*-Pt** in THF-water mixed solution (f_w = 95%) S21
Figure S21. Simulated and experimental CD spectra of ***R*-Pt** S22
Figure S22. Molecular orbitals of ***R*-Pt** related to the excitation listed in Table S3 S25

Table S1. Crystallographic data for ***R*-Pt** and ***S*-Pt** S11
Table S2. Spectroscopic data for ***R*-Pt** and ***S*-Pt** S23
Table S3. Selected TD-DFT calculated excitation energies for ***R*-Pt** S24

General Information

All reagents and solvents and were of the commercial reagent grade and were used without further purification unless otherwise noted. [Pt(II)(bpy)Cl_2] was prepared according to literature method[1].Dry MeOH was obtained by distillation over calcium hydride. Tetrahydrofuran (THF) was distilled from sodium benzophenone ketyl under a nitrogen atmosphere prior to use. CH_2Cl_2 and Toluene were distilled from CaH_2. CH_3CN for spectroscopy was purchased from Kanto Chemical co., inc. Solvent for PL and PL quantum yield measurements were deaerated by freeze degassing. ^1H and ^{13}C NMR spectra were recorded on a BRUKER AVANCE III 500 at 25 °C in d_6-DMSO. ^1H NMR chemical shifts are expressed in parts per million (δ) relative to trimethylsilane (TMS) as a reference. Matrix-assisted laser desorption ionization-time of flight (MALDI-TOF) mass spectroscopy (MS) spectra were recorded with a AB SCIEX 4800 MALDI TOF/ TOF analyzer, using 1,8-dihydroxy-9[10*H*]-anthracenone (dithranol) as the matrix.

Spectroscopy

UV-vis absorption spectra of CH_3CN solutions (1.0×10^{-5} M) and PMMA films were recorded with JASCO V-570 UV/VIS/NIR spectrometer. CD spectra of CH_3CN solutions (1.0×10^{-5} M) and PMMA films were recorded with JASCO J-720W spectrometer. Photoluminescence (PL) spectra of CH_3CN, CH_2Cl_2, toluene, and THF solutions (1.0×10^{-5} M), THF-water mixed solutions (1.0×10^{-4} M), solid state (powder samples) and PMMA films were acquired using JASCO FP-8600 spectrometer in air at room temperature, at excitation wavelength of 250 nm (solutions), 400 nm (powder samples and THF-water mixed solutions), and 380 nm (PMMA films). CPL spectra of THF-water mixed solutions (1.0×10^{-4} M), powders and PMMA films were measured with a JASCO CPL-300 spectrofluoropolarimeter at room temperature, at a scattering angle of 0° upon excitation with unpolarized, monochromated incident light with a 10 nm bandwidth for the PMMA films and 100 nm bandwidth for the powder samples. Absolute PL quantum yields of powders and PMMA films were determined using a JASCO PF-6500 spectrometer with an integrating sphere (JASCO ILF-533, diameter 96 mm) at excitation wavelength of 500 nm (powder samples) and 380 nm (PMMA films). The measurement of quantum yields of powder samples was performed by using KBr plates. Powders were placed between KBr plates and pressure of 20 MPa was applied. Fluorescence/Phosphorescence lifetimes were measured for powder samples and PMMA films with a HORIBA DeltaFlex spectrometer with a 370 nm LED light source for excitation. A colloidal silica suspension in water was used as a scatterer to determine the instrumental response. Dynamic light scattering spectra were measured for THF-water mixed solution (f_w = 95%) with Zetasizer Nano Series ZEN3600. For the optical measurements of solutions, a conventional 1 cm quartz cell was used.

Preparation of powder samples and PMMA films for the spectroscopy

Solid state samples (powder samples) for the spectroscopic measurements were prepared by dropping the MeOH suspension of the Pt complex on the glass substrate. The MeOH solvent was allowed to evaporate spontaneously. Samples dispersed in PMMA films were prepared by casting $CHCl_3$ solution of the Pt complex on the glass substrate. The ratio of the Pt complex to PMMA was 1 wt%, 2 wt% and 5 wt%, and the concentration of the Pt complex in $CHCl_3$ solution of PMMA/Pt complex was 0.63 M (1 wt%), 1.25 M (2 wt%) and 3.14 M (5 wt%). Thickness of the PMMA film was 160 mm for ***S*-Pt** and 190 mm for ***R*-Pt**.

X-ray Crystallography

Single crystals of ***R*-** and ***S*-Pt** were mounted on a glass fiber with paraton oil. Diffraction data were collected at 100 K on a Bruker SMART APEX II diffractometer fitted with a CCD-type area detector, and a full sphere of data was collected using graphite-monochromated Mo Kα radiation (λ = 0.71073 Å). Data frames were integrated with the Bruker SMART APEX III software and merged to give a unique data set for structure analysis. Numerical absorption correction by integration was applied on the basis of measured indexed crystal faces using SADABS program. The structures were solved by direct methods and refined by the full-matrix least-squares method on F^2 data with the SHELXL-2016/6 package. All non-hydrogen atoms were refined with anisotropic thermal parameters. Hydrogen atoms were included in calculated positions and refined with isotropic thermal parameters riding on those of the parent atoms. Crystallographic data and structure refinement details are listed in Table S1.

Theoretical calculation

All calculations were performed by using Gaussian 16 rev C.01 program package.[2] The initial geometry was taken from the X-ray crystal structure analysis and optimized by the density functional theory (DFT) at the level of CAM-B3LYP/Def2SVP for all atoms with the conductor-like polarizable continuum model (CPCM) to consider the solvent (CH_3CN). The time-dependent density functional theory (TD-DFT) calculation for ***R*-Pt** was conducted at the level of CAM-B3LYP/Def2SVP for all atoms with the conductor-like polarizable continuum model (CPCM) to consider the solvent (CH_3CN). The UV-vis absorption spectrum of ***R*-Pt** was simulated based on the 200 of the calculated oscillation strengths with Gaussian distribution with a bandwidth of 0.33 eV, and the spectrum was shifted by –0.29 eV to compensate the error of the CAM-B3LYP functional. The CD spectrum of ***R*-Pt** was also simulated based on the 200 of the calculated rotational strengths with Gaussian distribution with a bandwidth of 0.24 eV, and the spectrum was shifted by –0.29 eV to compensate the error of the CAM-B3LYP functional. Representative calculated singlet vertical excitation energies with relatively large oscillation strengths in acetonitrile are summarized in Table S3 and corresponding molecular orbitals are depicted in Fig. S22.

General procedure for synthesis of *R*- and *S*-Pt

The synthesis of ***R*-Pt** is representative. A mixture of [Pt(II)(bpy)Cl_2] (102 mg, 0.24mmol), (*R*)-BINOL (74 mg, 0.25 mmol), and K_2CO_3 (72 mg, 0.52 mmol) in methanol (20 ml)was refluxed under nitrogen atmosphere for overnight. After filtration of the resulting reddish solution through Celite, the filtrate was concentrated in vacuo. Purification of the product with silica gel column chromatography by using $CHCl_3$-MeOH (9 : 1) as an eluent, and then slow evaporation of $CHCl_3$ from the solution gave 52 mg (0.082 mmol) (34% yield) of ***R*-Pt** as a red crystal.

(*R*)-[Pt(II)(BINOL)(bpy)] (***R*-Pt**). ^{1}H-NMR (500 MHz, d_6-DMSO): δ 9.36(2H, d), 8.52(2H, d), 8.39(2H, t), 7.89(2H, t), 7.77(2H, d), 7.69(2H, d), 7.40(2H, d), 7.15(2H, t), 7.04(2H, t), 6.79(2H, d). ^{13}C-NMR (500 MHz, d_6-DMSO): 163.05, 157.15, 147.72, 140.09, 135.43, 128.67, 128.21, 127.92, 127.68, 125.65, 125.05, 125.00, 124.24, 123.54, 121.59. MS(MALDI-TOF): *m*/*z* 635.2 (M^+). Anal. calcd for $C_{30}H_{20}N_2O_2Pt$: C 56.69, H 3.17, N 4.41. Found: C 56.56, H 3.18, N 4.36.

(*S*)-[Pt(II)(BINOL)(bpy)] (***S*-Pt**). ^{1}H-NMR (500 MHz, d_6-DMSO): δ 9.36(2H, d), 8.52(2H, d), 8.39(2H, t), 7.89(2H, t), 7.77(2H, d), 7.69(2H, d), 7.40(2H, d), 7.15(2H, t), 7.04(2H, t), 6.79(2H, d). ^{13}C-NMR (500 MHz, d_6-DMSO): 163.05, 157.14, 147.71, 140.08, 135.43, 128.68, 128.21, 127.92, 127.68, 125.65, 125.05, 125.01, 124.24, 123.54, 121.59. MS(MALDI-TOF): *m*/*z* 635.2 (M^+). Anal. calcd for $C_{30}H_{20}N_2O_2Pt$: C 56.69, H 3.17, N 4.41. Found: C 56.56, H 3.16, N 4.40.

Scheme S1

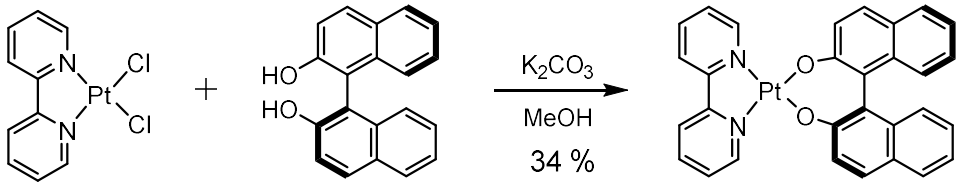

(*R*)-[Pt(BINOL)(bpy)]

Reference

[1] T. J. Egan, K. R. Koch, P. L. Swan, C. Clarkson, D. A. Van Schalkwyk, P. J. Smith, *J. Med. Chem*., 2004, **47**, 2926.

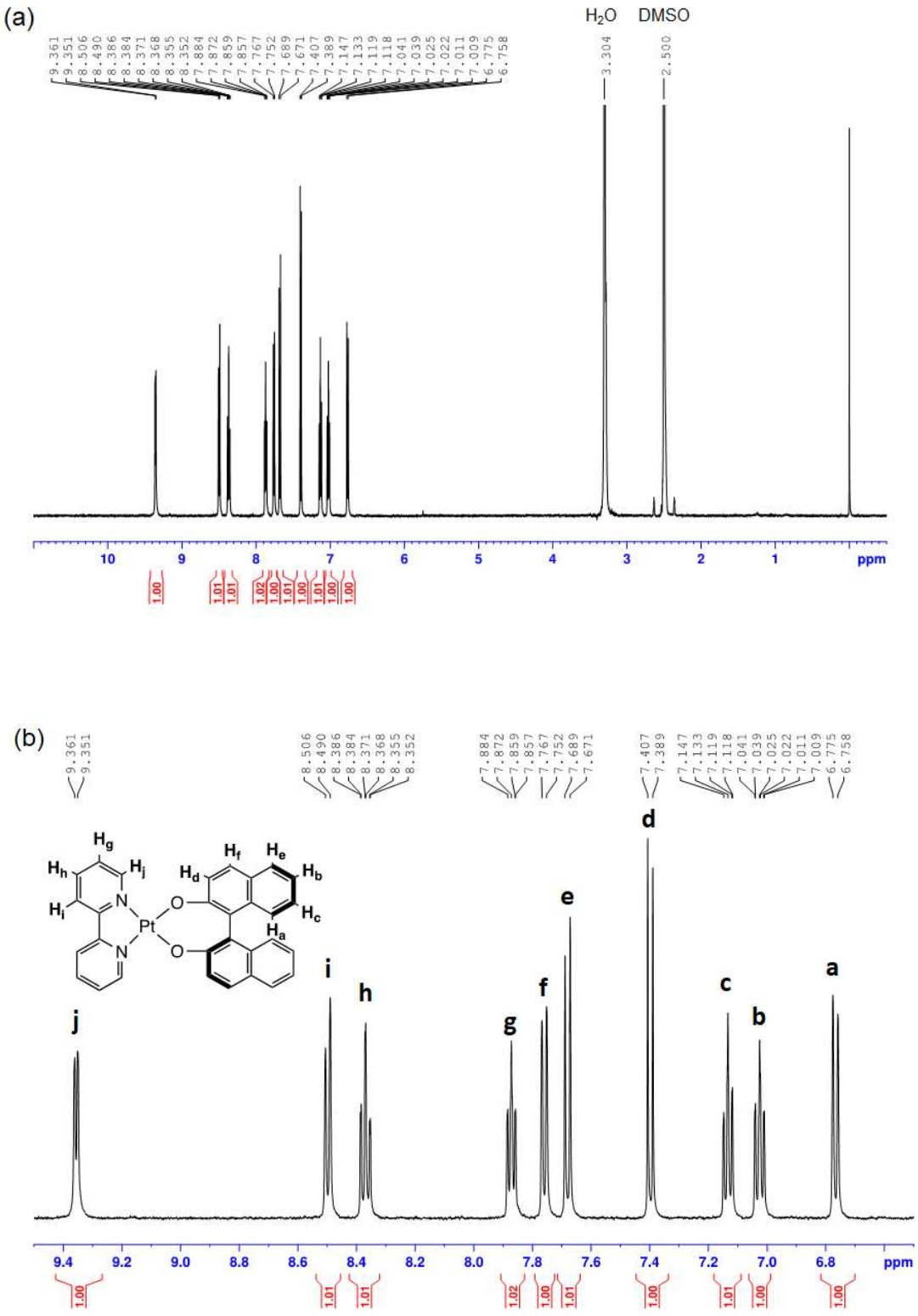

Figure S1. (a) ^{1}H-NMR spectrum of ***R*-Pt** (500 MHz, d_6-DMSO, 298 K, Me_4Si) and (b) expanded NMR spectrum of ***R*-Pt**

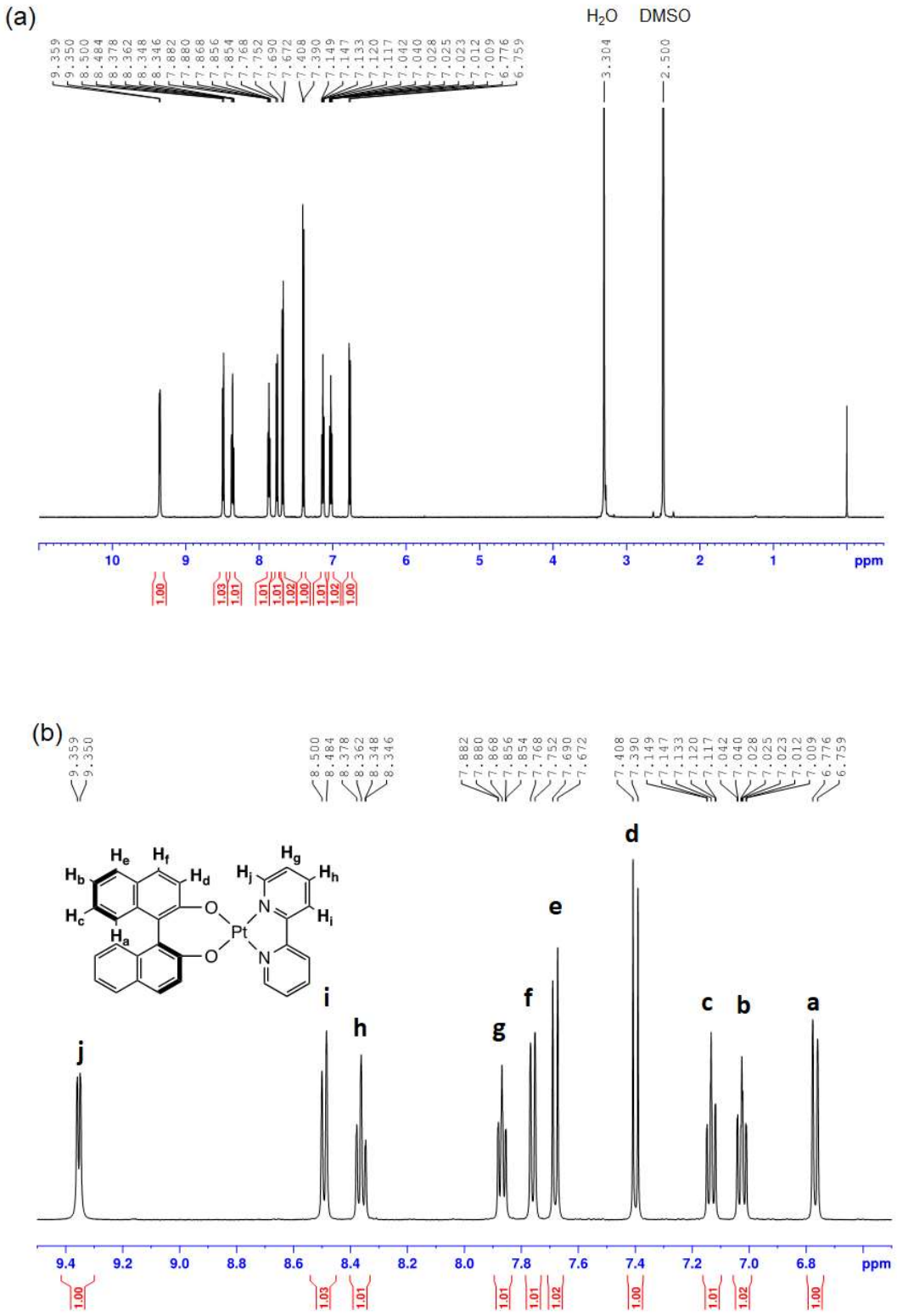

Figure S2. (a) ^{1}H-NMR spectrum of ***S*-Pt** (500 MHz, d_6-DMSO, 298 K, Me_4Si) and (b) expanded NMR spectrum of ***S*-Pt**

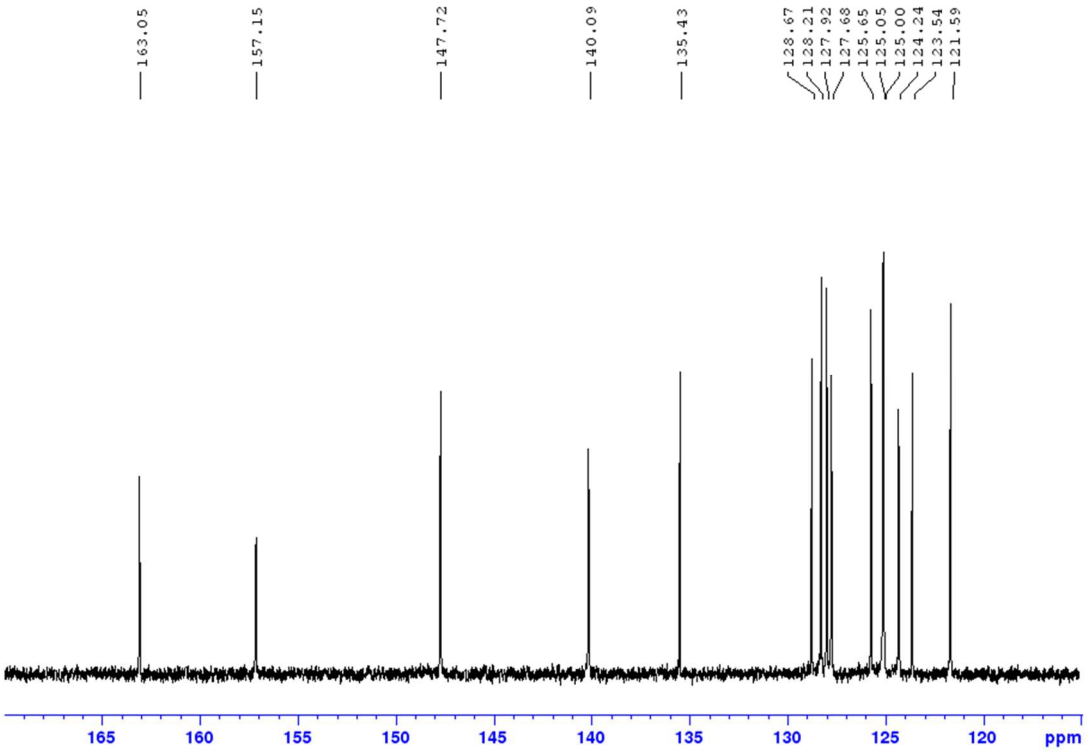

Figure S3. ^{13}C-NMR spectrum of ***R*-Pt** (500 MHz, d_6-DMSO, 298 K, Me_4Si)

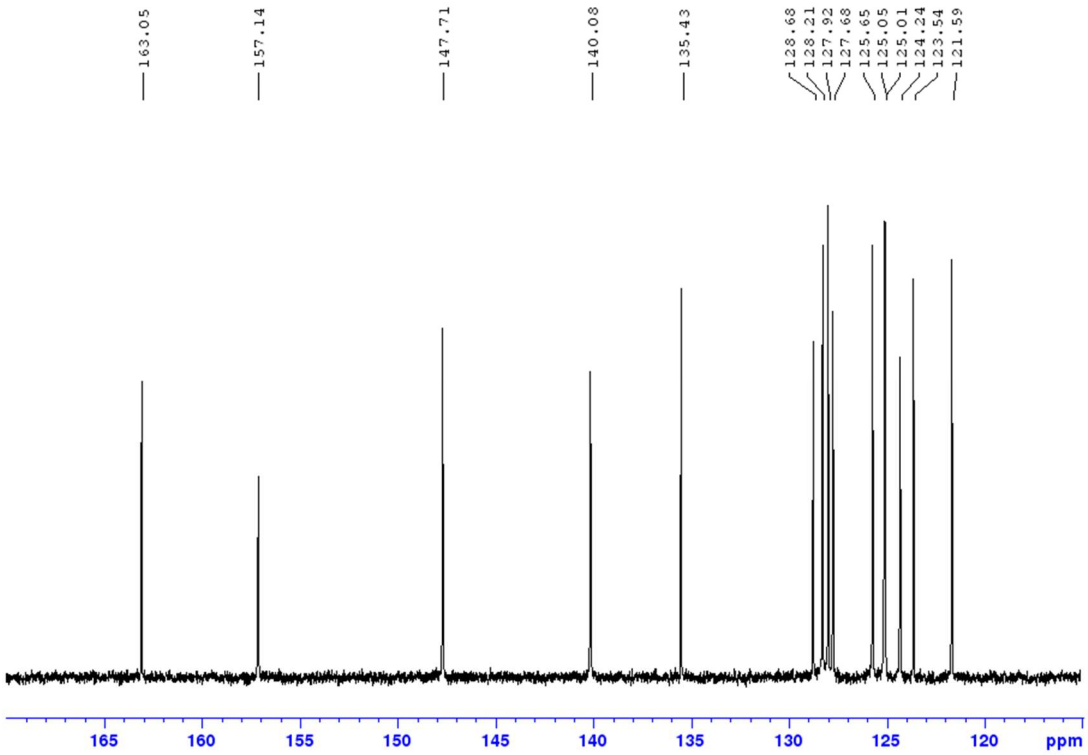

Figure S4. ^{13}C-NMR spectrum of ***S*-Pt** (500 MHz, d_6-DMSO, 298 K, Me_4Si)

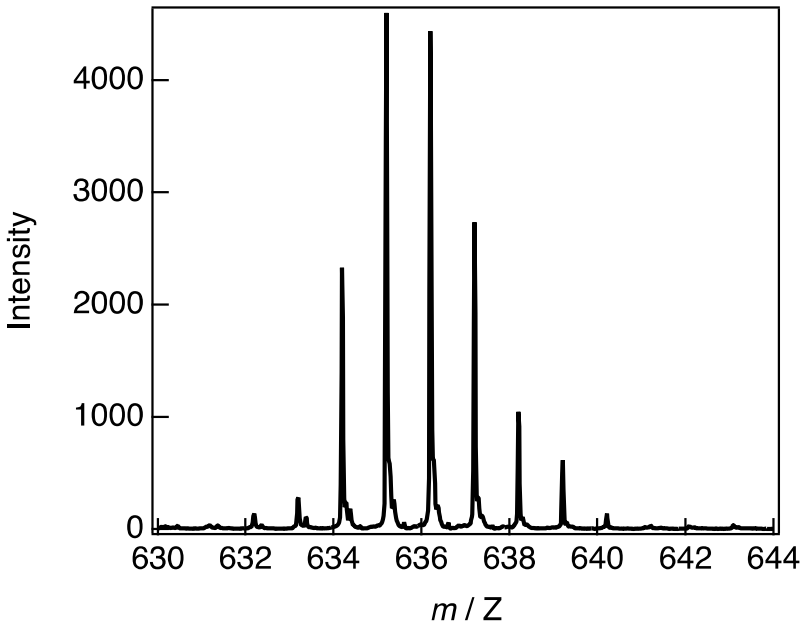

Figure S5. Mass spectrum of ***R*-Pt**

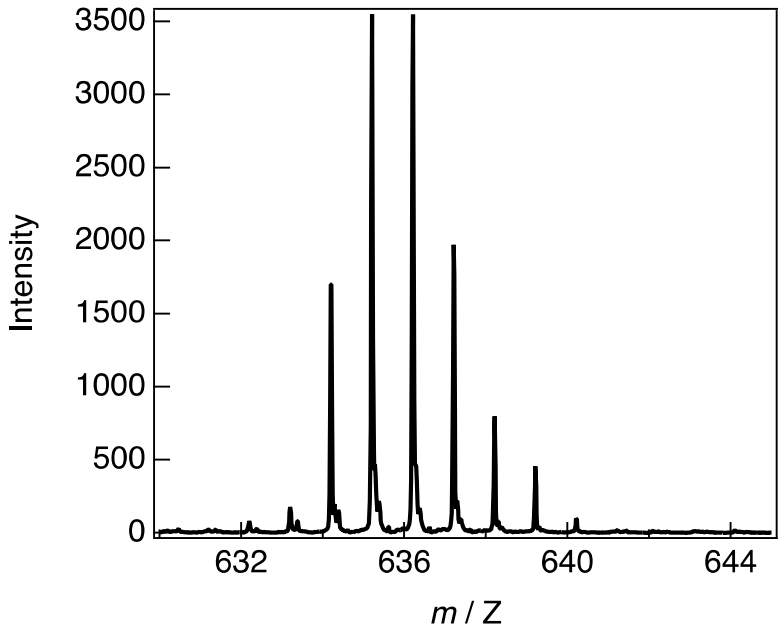

Figure S6. Mass spectrum of ***S*-Pt**

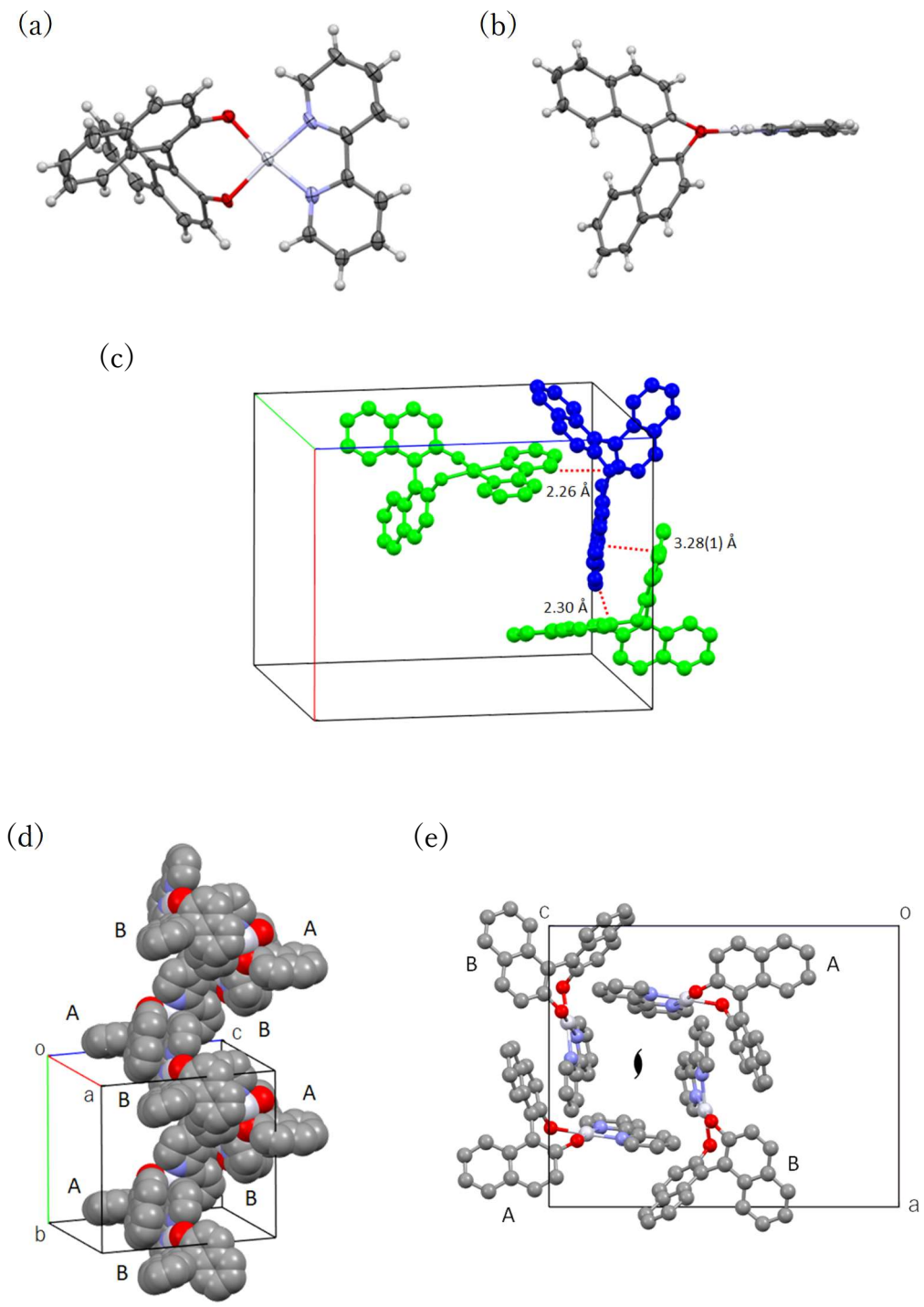

Figure S7. Crystal structure of ***S*-Pt**. (a) top view and (b) side view of molecular structure. The dihedral angles between the two naphthyl groups are almost 72°. (c) Intermolecular interactions. Helical assembly of ***S*-Pt**. (d) Projected perpendicular to stacking direction and (e) projected along b-axis. H atoms are omitted in (d) and (e) for clarity.

Table S1. Crystallographic data for ***R*-Pt** and ***S*-Pt**.

	***R*-Pt**	***S*-Pt**
Formula	$C_{30}H_{20}N_2O_2Pt$	$C_{30}H_{20}N_2O_2Pt$
Formula weight	635.57	635.57
Color	Red	Red
Crystal size/ mm	0.150 × 0.140 × 0.100	0.330 × 0.070 × 0.050
Crystal system	Orthorhombic	Orthorhombic
Space group	$P2_12_12_1$	$P2_12_12_1$
a (Å)	14.9659(16)	14.959(2)
b (Å)	17.1787(18)	17.171(3)
c (Å)	18.703(2)	18.707(3)
V(Å^3)	4808.3(9)	4805.1(13)
Z	8	8
F(000)	2464	2464
D_{calc} (g/cm^3)	1.756	1.757
Abs coeff (mm^{-1})	5.867	5.871
R_1[a] ($I > 2\sigma(I)$)	0.0283	0.0313
R_w[b] ($I > 2\sigma(I)$)	0.0595	0.0621
R_1[a] (all data)	0.0319	0.0391
R_w[b] (all data)	0.0617	0.0665

[a] $R_1 = \sum \| |F_0| - |F_c| \| / \sum |F_0|$ $for\ I > 2\sigma(I)$ data

[b] $R_w = \left\{ \sum w \left(|F_0| - |F_c| \right)^2 / \sum w |F_0|^2 \right\}^{1/2}$

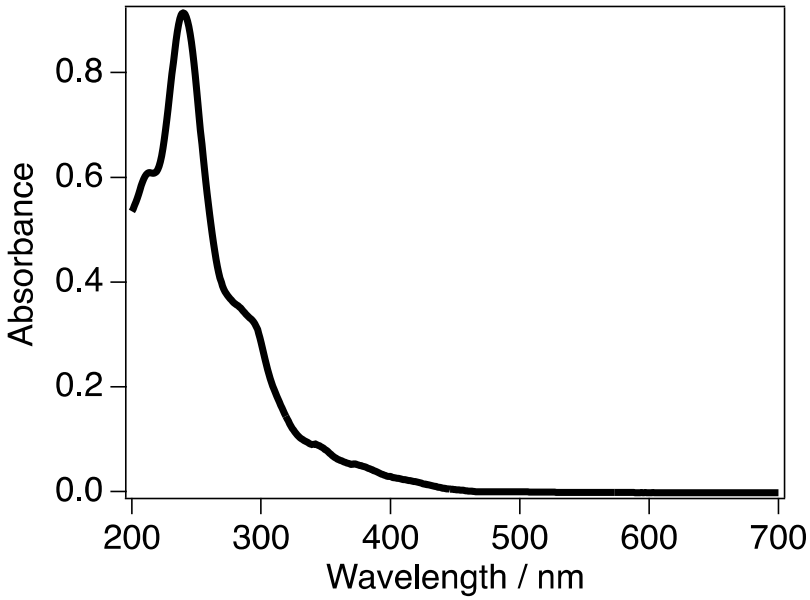

Figure S8. Absorption spectrum of ***S*-Pt** in acetonitrile solution (1.0×10^{-5} M)

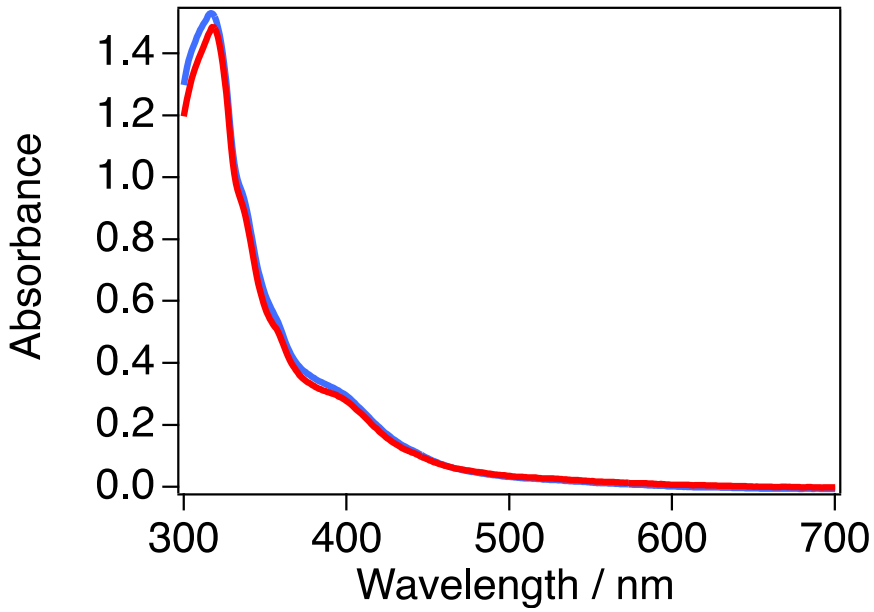

Figure S9. Absorption spectra of ***R*-Pt** (red line) and ***S*-Pt** (blue line) in PMMA films.

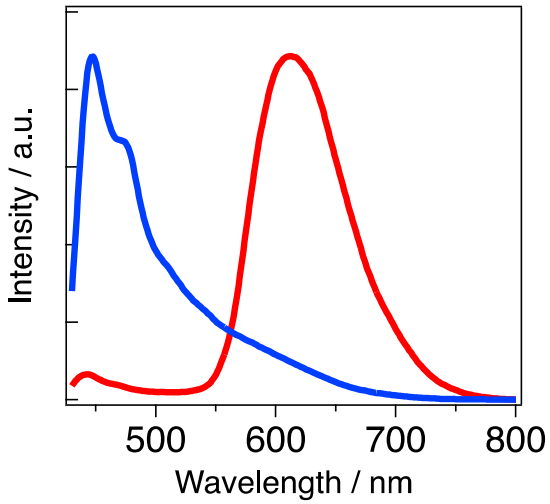

Figure S10. Emission spectra of ***S*-Pt** in powder (red) excited at 400nm and PMMA film (1 wt%) (blue) excited at 380nm.

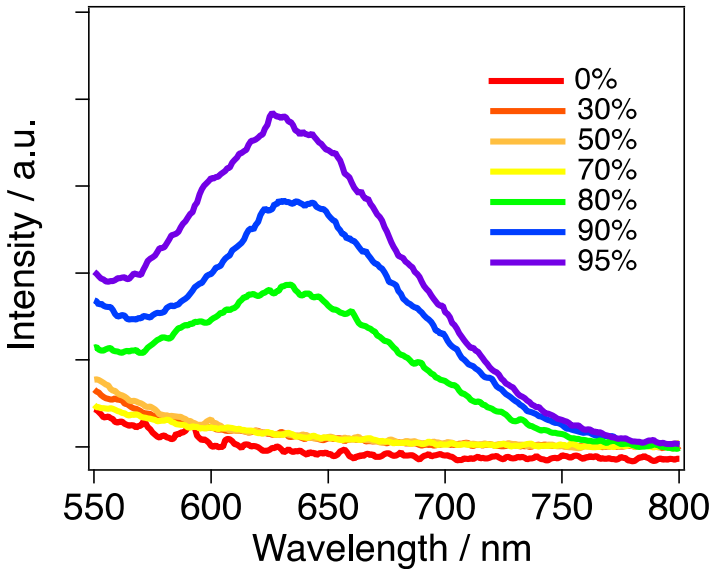

Figure S11. Emission spectra of ***R*-Pt** in THF-water with different volume fraction of water (1.0×10^{-4} M) excited at 400nm.

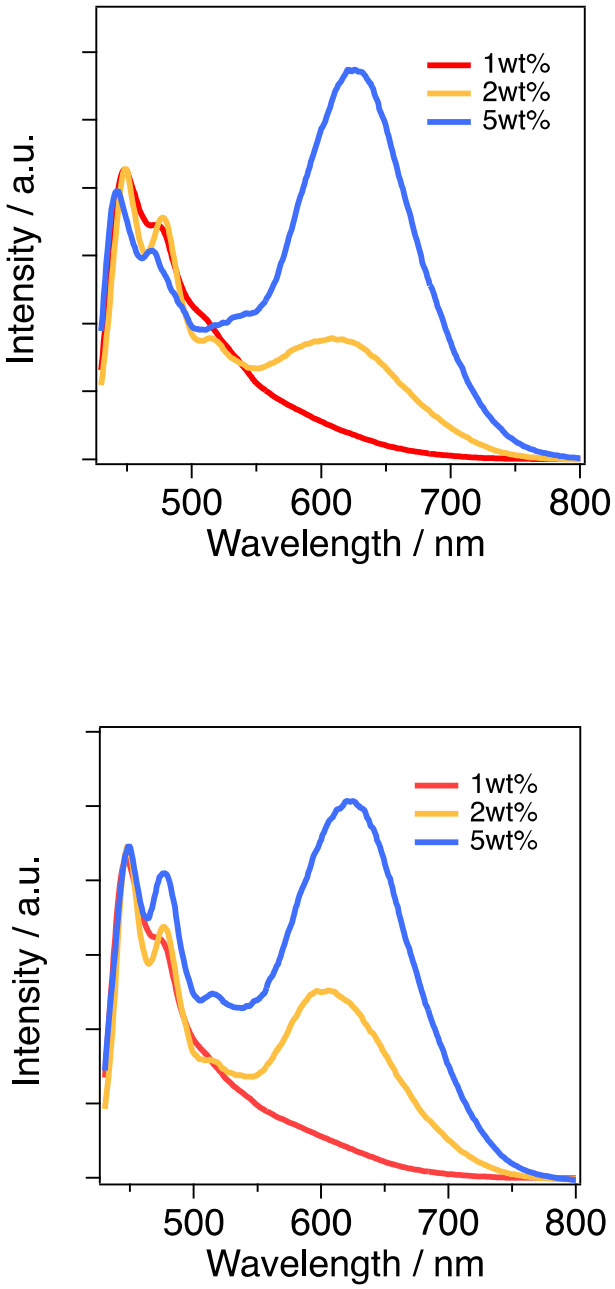

Figure S12. Emission spectra of ***R*-Pt** (upper) and ***S*-Pt** (lower) dispersed in the PMMA films with the concentration of 1 wt% (red), 2 wt% (yellow), and 5 wt% (blue) excited at 380 nm.

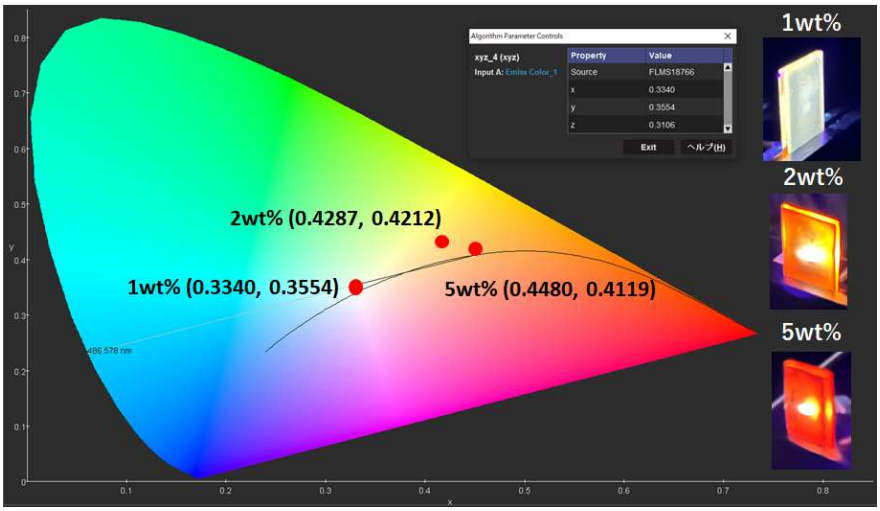

Figure S13. CIE (x, y) coordinates of ***S*-Pt** dispersed in PMMA films with the concentration of 1, 2, and 5 wt%.

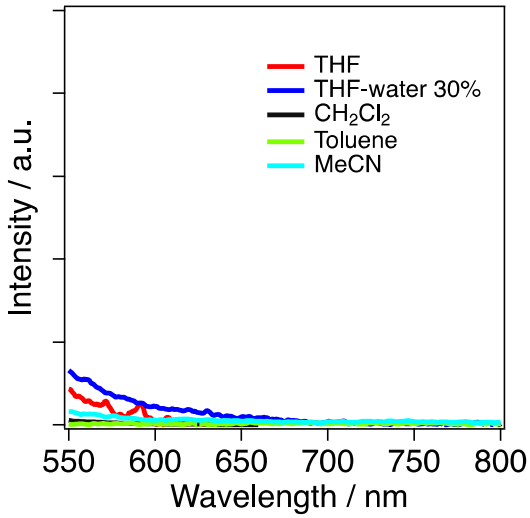

Figure S14. Emission spectra of ***R*-Pt** in THF, THF-water (fraction of water f_w = 30%), CH_2Cl_2, toluene, and CH_3CN in dilute condition [1.0×10^{-5} M except for THF (1.0×10^{-4} M)] excited at 250 nm for THF-water, CH_2Cl_2, toluene, and CH_3CN solutions and at 400 nm for THF solution.

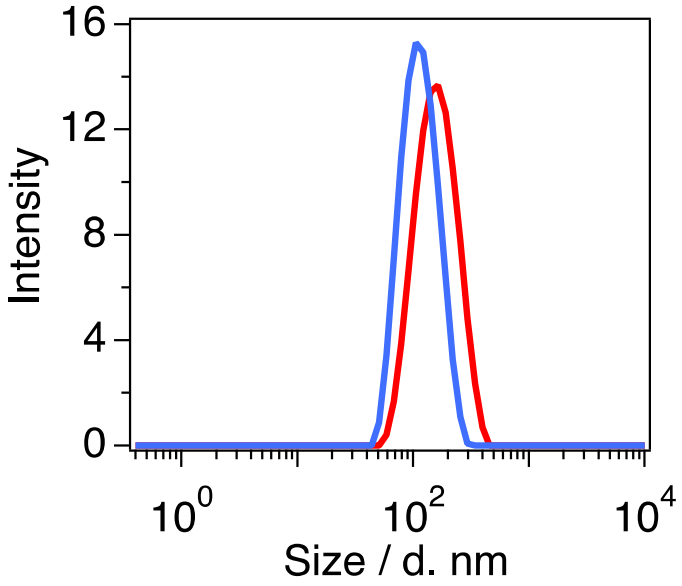

Figure S15. Dynamic light scattering profile of ***R*-Pt** (red) and ***S*-Pt** (blue) in THF-water mixed solution (fraction of water f_w = 95%).

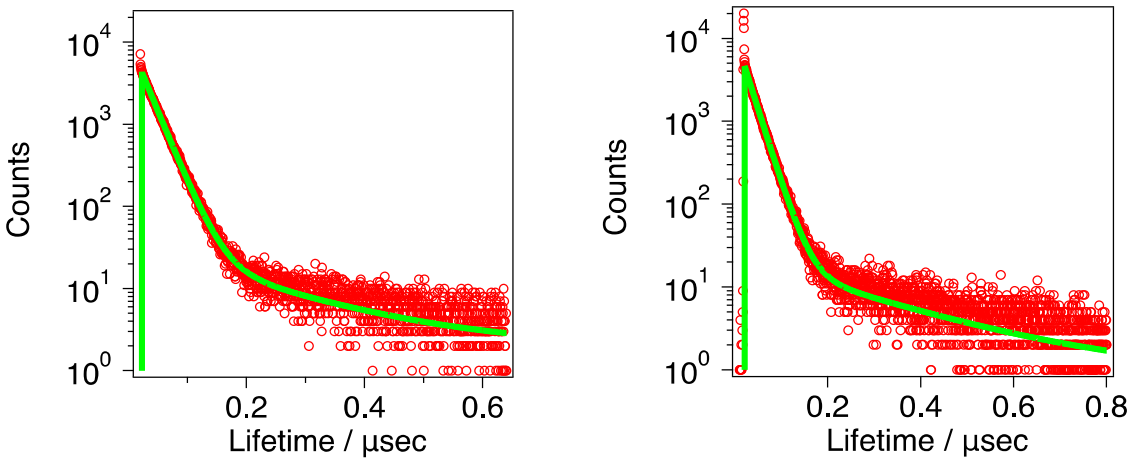

Figure S16. Emission decay profiles of ***R*-Pt** (left) and ***S*-Pt** (right) in powders excited at 455 nm and fit (green solid line).

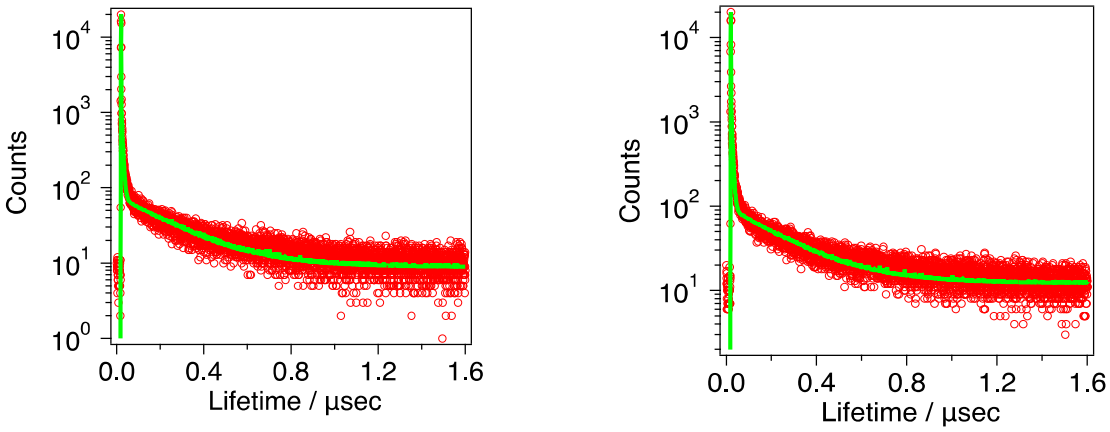

Figure S17. Emission decay profile of ***R*-Pt** (left) and ***S*-Pt** (right) in PMMA film (f_{Pt} = 1 wt%) excited at 370 nm and fit (green solid line).

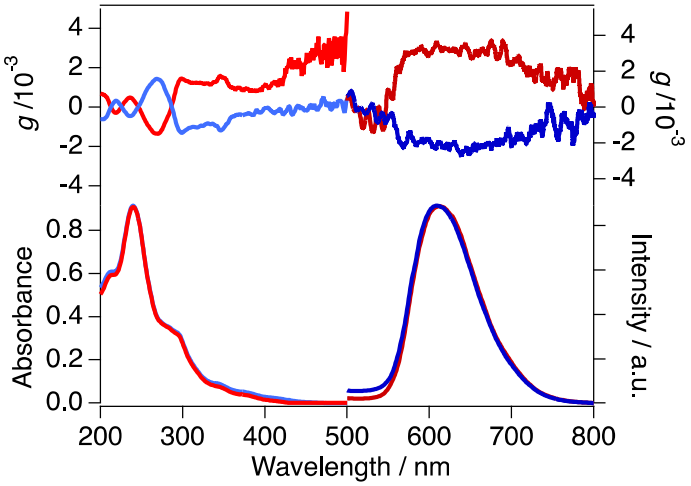

Figure S18. g_{abs} (upper left) and UV-vis spectra (lower left) in acetonitrile (1.0×10^{-5} M), and g_{CPL} (upper right) and emission spectra (lower right) in powder excited at 400 nm of ***R*-Pt** (red) and ***S*-Pt** (blue).

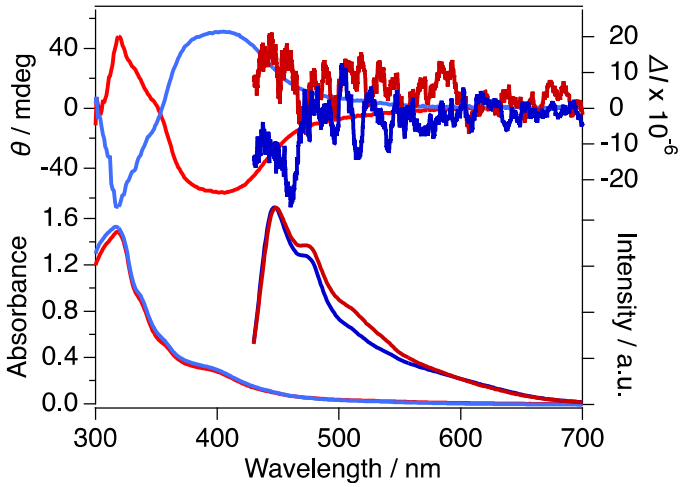

Figure S19. CD and CPL spectra (upper) and UV-vis and emission spectra (lower) of ***R*-Pt** (red) and ***S*-Pt** (blue) in PMMA films (1 wt%). The PMMA films were excited at 380 nm

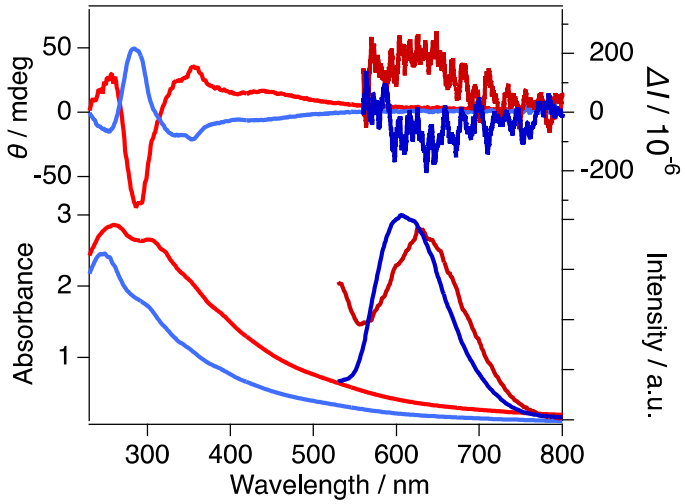

Figure S20. CD and CPL spectra (upper) and UV-vis and emission spectra (lower) of ***R*-Pt** (red) and ***S*-Pt** (blue) in THF-water mixed solution (fraction of water f_w = 95%) The mixed solutions were excited at 400 nm.

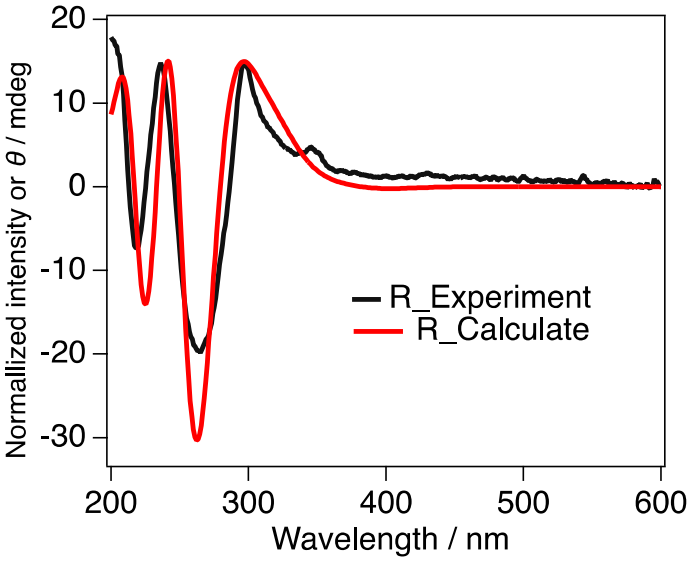

Figure S21. Simulated CD spectrum (red) of ***R*-Pt** by TD-DFT calculation with the experimental spectrum (black).

Table S2. Spectroscopic data of powder, PMMA film (1 wt%), and CH_3CN solution of ***R*-Pt** and ***S*-Pt**.

	sample	***R*-Pt**	***S*-Pt**
Quantum yield	Powder (λ_{ex} = 500 nm)	0.46%	0.55%
	PMMA film (λ_{ex} = 380 nm)	0.085%	0.14%
Lifetime	Powder (λ_{ex} = 455 nm, λ_{det} = 612 nm)	24 ns (96%) 0.24 μs (4%)	25 ns (95%) 0.18 μs (4%)
	PMMA film (λ_{ex} = 370 nm, λ_{det} = 500 nm)	0.67 ns (52%) 8.3 ns (16%) 0.27 μs (33%)	0.71 ns (52%) 7.7 ns (16%) 0.26 μs (32%)
g_{abs}[a]	CH_3CN soln. (1.0×10^{-5} M)	-1.4×10^{-3}	1.4×10^{-3}
	PMMA film	-2.3×10^{-3}	3.5×10^{-3}
g_{cpl}	Powder (λ_{ex} = 400 nm)	3.4×10^{-3}	-2.3×10^{-3}
	PMMA film (λ_{ex} = 380 nm)	1.3×10^{-3}	-2.4×10^{-3}

[a] g_{abs} values were estimated at 270 nm (CH_3CN solution) and 385 nm (powder).
[b] g_{cpl} values were estimated at 621 nm (powder) and 459 nm (PMMA film)

Table S3. Selected TD-DFT calculated excitation energies corresponding to the experimental absorption wavelengths and main weights of transitions for ***R*-Pt**.

Excited state	Experiment (nm)	Excitation Energy (shifted by –0.29eV, nm) (Oscillation strength)	Transitions (% weight)
1	440	438 (0.0011)	122 → 125 (11) 124 → 125 (75)
2	380	388 (0.0141)	122 → 128 (5) 122 → 130 (7) 124 → 128 (56) 124 →130 (7)
4	350	359 (0.1579)	119 → 125 (32) 123 → 125 (50)
17	280-290	287 (0.2633)	116 → 125 (74) 124 → 126 (7)
18		285 (0.1456)	121 → 128 (16) 123 → 128 (36) 124 → 131 (18)
31	240	242 (0.9171)	121 → 128 (21) 122 → 130 (8) 123 → 130 (21)
35		237 (0.2236)	113 → 125 (22) 114 → 125 (18) 119 → 126 (13)
37		234 (0.3910)	122 → 128 (16) 123 → 131 (22) 124 → 133 (26)

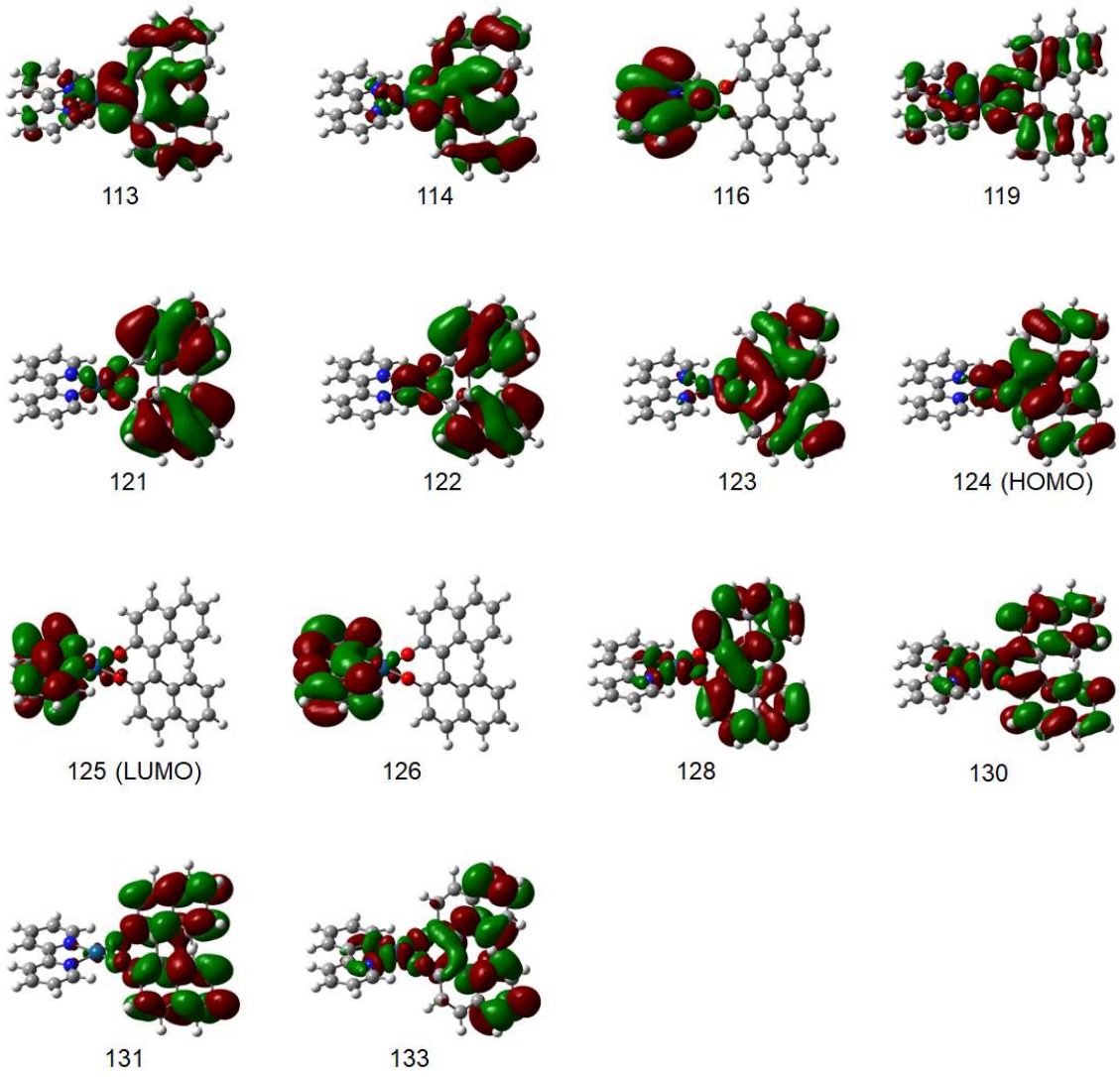

Figure S22. Molecular orbitals of ***R*-Pt** related to the excitation listed in Table S3